Bounding the localized to ductile transition in porous rocks: implications for geo-reservoirs

Gabriel G. Meyer[1,*] and Marie Violay[1]

[1]LEMR ENAC, Ecole Polytechnique Fdrale de Lausanne, CH

[*]Corresponding author: gabriel.meyer@epfl.ch

Abstract

Porous rocks have long been the focus of intense research driven by their importance in our society as host to our most essential resources (oil, gas, water, geothermal energy, etc), yet their rheology remains poorly understood. With increasing depth, porous rocks transition from being brittle (dilational deformation leading to localized failure) to being ductile (homogeneous compactive flow, no failure). The transition between these two regimes is crucial for reservoir engineering. In fact, brittle, localized deformation of porous rocks is generally accompanied by permeability enhancement but also induced seismicity, while ductile deformation leads to aseismic permeability reduction. Decades of experimental work has shown that this transition is not sharp but rather spans a wide P, T domain,

but to this day, no clear boundaries have been established. Here, we subjected pre-faulted samples of volvic trachyandesite to increasing confining pressure, deforming the samples each pressure step and recording strain partitioning between off-fault bulk deformation and on-fault slip. For the first time, we show that the localized-to-ductile transition (LDT) in porous rocks is bound by the stress criterion $\sigma_{\mathrm{y}} < \sigma_{\mathrm{f}} < \sigma_{\mathrm{flow}}$. Additionally we show that, in this regime, once both fault sliding and bulk flow are active, the partitioning of strain between the two can be described by the empirical ratio: $(\sigma_{\mathrm{f}} - \sigma_{\mathrm{y}})/(\sigma_{\mathrm{flow}} - \sigma_{\mathrm{y}})$. Finally, we propose a critical stress representation that takes into account the existence of the LDT in porous rocks.

Keywords: Geomechanics, Permeability and porosity, Fracture and flow

1 Introduction

Most of the shallow crust is comprised of porous rocks which are crucial in our economy since they contain critical resources such as gas, oil, water as well as being potential hosts for underground storage (e.g., CO_2).

With increasing pressure and temperature, porous rocks transition from cataclastic faulting to compactive cataclastic flow (Wong and Baud, 2012). This transition is accompanied by a change in deformation mode, from strain being localized on faults to strain being distributed (ductile).

The localized-ductile transition (LDT) in porous rocks is a topic of

outmost importance for the aforementioned geo-energy applications, since it controls the global behaviour of reservoirs. This includes faulting and the formation of compaction bands (Aydin and Johnson, 1978; Underhill and Woodcock, 1987; Shipton and Cowie, 2001; Scott and Nielsen, 1991), the coupling between strain localization and reservoir hydraulic properties (Antonellini and Aydin, 1994; Fowles and Burley, 1994), reservoir compaction and subsidence (Fisher et al., 1999; Makowitz and Milliken, 2003), borehole instability and well failure (Veeken et al., 1989; Fredrich et al., 2000; Coelho et al., 2005), seismic attenuation (Yarushina and Podladchikov, 2010) and induced earthquakes (Scholz, 2019; Grigoli et al., 2017; Schultz et al., 2020).

Under cool shallow crust conditions, deformation of porous rocks is accomodated through dilational micro-cracking (i.e., dilatancy) which eventually leads to cataclastic failure along a fault plane. Deeper, under greater pressure and temperature, dilational deformation gives way to compactive cataclastic flow whereby the collapse of pores and/or the crushing of grains leads to a homogeneous deformation of the rock (Wong et al., 1997; Paterson and Wong, 2005; Wong and Baud, 2012; Heap and Violay, 2021; Jefferd et al., 2021). In the compactive ductile regime, the crushing of grains or collapse of pores can lead to the formation of compaction bands which, despite being highly localized processes (strain is concentrated on mm thick bands), lead to a somewhat homogeneous

deformation at the sample scale without failure and for this reason they are widely considered by the community to be ductile (Brantut et al., 2014). It has long been recognized that the boundary between these two deformation regimes is all but a sharp limit. However, and despite its importance for reservoir engineering, the LDT has never been accurately bound in porous rocks.

In tight rocks such as Carrara marble (with initial porosity of 0.5%), the LDT is bound by a stress criterion and occurs under the conditions where :

$$\sigma_{\mathrm{y}} \ < \ \sigma_{\mathrm{f}} \ < \ \sigma_{\mathrm{flow}}, \tag{1}$$

where σ_{y} is the yield stress (i.e., stress at the onset of inelastic deformation) of the bulk rock, σ_{f} is the fault frictional strength and σ_{flow} is the maximum stress the bulk rock can support (Meyer et al., 2019). Furthermore, it was shown that the LDT in tight rocks is gradual and that there exists a zone in the crust where both delocalized bulk strain coexists with on-fault localized strain and that their respective contributions to the total deformation is proportional to the ratio:

$$\frac{\sigma_{\mathrm{f}} - \sigma_{\mathrm{y}}}{\sigma_{\mathrm{flow}} - \sigma_{\mathrm{y}}}, \tag{2}$$

(Meyer et al., 2019).

In light of this, one can wonder whether the LDT in porous rocks is bound by the same stress criteria as that in tight rocks, and if so, where the

compaction processes fit within the boundaries.

Before proceeding, a note has to be made about the vocabulary surrounding this rheological transition, otherwise colloquially referred to as brittle-ductile transition, or BDT. This lexicon is infamous for being equivocal and has been the source of misunderstanding in the community. To remedy this problem, Rutter (1986) proposed a generally accepted nomenclature to which we will strictly adhere in the present work (Figure 1). The first, and possibly most contentious, point of Rutter (1986) is that "[e]veryone will agree that brittleness is associated with the formation of cracks, and can therefore be defined at the microscopic level. It is essentially a mechanistic concept." Similarly, they argue that the concept of ductility should not be dependent on mechanism of deformation but should remain a strict description of mode of failure (i.e., degree of deformation homogeneity). In this definition, "[...] brittleness and ductility can occur together, and the terms should not be used in a mutually exclusive way". For this reason, we will restrict our use of the term "brittle" to describe cracking at the grain scale (i.e., pressure dependent mechanisms), to which we will generally prefer the less contentious counterpart of "cataclastic". On the other hand, processes involving pressure-independent mass transfer and/or crystal lattice distorsion will be referred to as "crystal-plastic". "Ductile" will be used to describe homogeneous deformation at the sample scale and will be opposed

to "localized" or "faulting" when describing strain localization. The term "brittle-ductile transition" or "BDT", despite being imprecise, has now permeated the literature to the extent that it is impossible not to use it in the present article. When compelled to do so, we will use quotation marks to indicate its more conceptual value rather than referring to an actual transition. In all instances where a complete description is possible, we will use detailed expressions such as "cataclastic faulting to crystal plastic flow transition" etc.

In the framework of this nomenclature, it is clear that what is colloquially referred to as the "BDT" is actually comprised of two distinct transitions, each with their own distinct boundaries: a transition in how strain is accommodated macroscopically regardless of its micro-mechanistic nature, from being localized (faulting) to being ductile (homogeneous; Meyer et al. (2019)), and another micro-mechanical transition in what accommodates strain, from micro-cracking of grains (brittle/cataclastic processes) to crystal plasticity. Therefore, there can exist a region in the crust where the deformation is fully cataclastic (no crystal plasticity) but fully ductile (no localization) and vice-versa (e.g., Tullis and Yund (1992)). The nature of the microprocesses accommodating strain in a deforming rock (cataclastic vs plastic) as well as the mode of deformation (localized vs ductile) is a key control on its properties such as strength, porosity, permeability; as well as its seismic potential. For this reason, it is critical to systematically

distinguish the two transitions.

The present study focuses on the first of the two transitions: the transition in deformation mode or localized-to-ductile transition. To investigate the LDT in porous rocks, we conducted a series of three experiments on cores of a porous lava. We subjected the samples to incrementally higher confinements and recorded strain partitioning as they transitioned from being fully localized to being fully ductile. While ours is not the most representative reservoir rock, it serves the purpose of establishing whether the LDT occurs in porous rocks and whether it follows the pre-established boundaries observed for low-porosity rocks. Building on our observations, we then extend our discussion to sandstones and limestones by using extensive published experimental data and show that the boundaries observed in a porous volcanic rock are applicable to all porous lithologies. We finally propose a new representation of critical stress envelopes accounting for our observations.

2 Sample and methods

For this study, we selected a trachyandesite from the Chane des Puys, a 40 km-long chain of cinder cones, lava domes, and maars in the Massif Central of France. We chose Volvic trachyandesite as it is a well studied rock. Its porosity was determined to be 21% using the double weight water saturation method (Heap et al., 2022). Its microstructure consist of

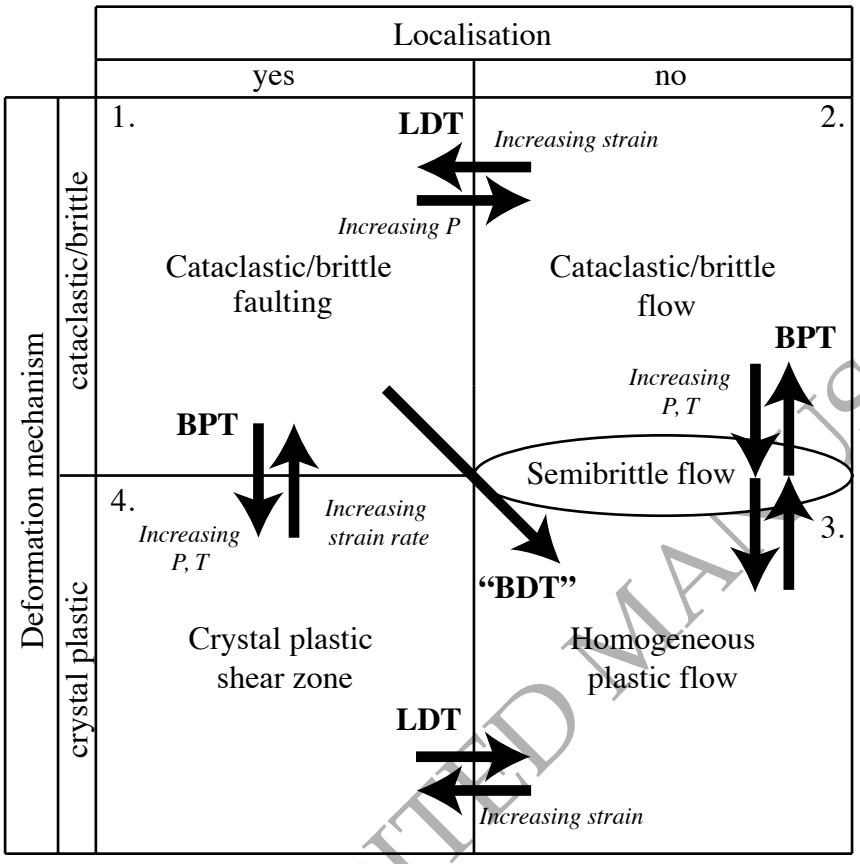

Figure 1: Adapted version of the nomenclature established by Rutter et al., 1986. Arrows represent possible transitions with their associated names. Where possible, the conditions under which these transitions can occur are specified in italics. LDT: localized-ductile transition; BPT: brittle-plastic transition; BDT: brittle-ductile transition.

irregularly shaped pores (average equivalent pore radius $< 10\mu$m) embedded in a microcrystalline groundmass with a slight pore shape preferred orientation (10-15% of pores have aspect ratios < 0.7; Louis et al. (2007); Heap et al. (2022)). Moreover, it has recently been the subject of a thorough study based on the same triaxial apparatus as that used in the present study which explored its brittle-ductile behaviour, adding some interest for reproducibility (Heap et al., 2022).

Cylindrical cores of 38×80 mm were cored from a single block sourced from Puy de la Nugre, near the town of Volvic, and their surfaces were rectified to ensure parallelism within ± 100 μm.

Experiments were carried on FIRST, an oil confining, triaxial apparatus located at the Laboratory of Experimental Rock Mechanics (LEMR) at Ecole Polytechnique Federale de Lausanne (EPFL), Switzerland, see details in Cornelio and Violay (2020); Nol et al. (2019, 2021).

Samples were oven dried at 60 °C for 24 hours prior to being fitted with four pairs of 120 Ω strain gauges (SG), four axial and four radial gauges, bonded onto the rock surface with superglue. Sample shortening was also recorded by a pair of linear variable differential transformers (LVDTs) present in the pressure vessel. Samples were then sandwiched between two thin layers of perforated Teflon paper to ensure lubrication of the loading surfaces, before the assembly was slid into a Viton jacket and placed within the pressure vessel.

A total of three experiments were conducted in the framework of this study. We tested the influence of strain rate on the LDT by conducting an experiment at 10^{-5} s^{-1} and another at 10^{-4} s^{-1}. Additionally, we investigated the influence of water on the LDT by conducting an experiment on a saturated sample at a constant strain rate of 10^{-5} s^{-1}. All experiments were carried-out at room temperature.

The experiments were divided in two distinct stages : a faulting stage identical for all experiments (labelled 1 in Figure 2 a.) and a cycling stage where the different experimental conditions were tested (labelled 2 in Figure 2 a.).

During the faulting stage, confining pressure (P_c) was increased to 5 MPa before the sample was loaded at a strain rate of 10^{-5} s^{-1} until sample-scale brittle failure was achieved. After failure, 0.1 mm of vertical shortening was accumulated on the fault and the differential stress (Q) subsequently removed at the same loading rate (10^{-5} s^{-1}).

During the cyclic loading stage, confining pressure was increased from 5 to 140 MPa by 20 MPa steps. Every step, the sample was loaded at a constant strain rate of 10^{-5} or 10^{-4} s^{-1} until about 0.2 mm irrecoverable, uncorrected (from machine deformation) strain was accumulated in the sample after which, the differential stress was fully removed at the same loading rate before proceeding to the following step.

Fault reactivation and strain partitioning were accessed by comparing the

average output of the axial strain gauges (which record local deformation, i.e., they do not record fault slip) and that of the two LVDTs (which record the total deformation), a method developed by Meyer et al. (2019). To do so, we subtracted the matrix strain (measured with strain gauges) from the total shortening (measured with external displacement transducers) and normalized it by the total shortening.

Given the random nature of brittle failure (no control on the fault position or angle in the sample), some SGs could be intersected by the fracture and destroyed during the faulting stage of the experiment. Moreover, with increasing confinement, the sensors are more prone to spontaneous mechanical failure (e.g., ruptured wires). If at any moment less than two gauges were to be functional, the experiment would be terminated.

In the experiment conducted under wet conditions, the sample was saturated with de-ionized water after the faulting stage. To do so, a pore pressure (P_p) of 5 MPa was applied on the top end of the sample while the bottom end was kept open to the atmosphere. The P_p gradient was maintained for 30 minutes after fluid flow was first observed at the bottom end of the sample, after what the pore fluid system was closed and P_p kept constant at 5 MPa on both ends of the sample with two high precision syringe pumps (Nol et al., 2021). During the two-hour duration of the experiment, we do not anticipate that any significant chemical fluid-rock interaction occurred.

3 Results

3.1 Mechanical data

An example of the typical mechanical data gathered during our experiments is shown in Figure 2. These data were gathered during the experiment conducted dry at a strain rate of 10^{-5} s^{-1}.

During the first stage of the experiment (i.e., faulting at $P_c = 5$ MPa), stress increases with total shortening, first linearly, before rolling over and suddenly dropping from around 120 MPa down to 55 MPa at 1.1% total shortening (Figure 2, a.). After this, stress plateaus at 50 MPa for the remainder of the first stage. This stress drop followed by a plateau corresponds to brittle failure of the sample followed by some residual friction on the created fault.

Similarly, during the first stage of the experiment, the average local strain (strain gauges output) increases linearly with total shortening (LVDT output) and with a slope of one up to maximum value around 1.1%, where the sample failed (Figure 2, b.). This failure translated into a sudden drop in average local strain by 0.4% followed by a plateau for the remainder of the stage.

During the first cycle at $P_c = 20$ MPa, stress first increases linearly with total shortening before rolling over at 93 MPa and eventually plateauing at 106 MPa. Concurrently, the average local strain initially shows a linear

increase with total shortening followed by a plateau. The end of the linear increase of stress with total shortening coincides with that of average local strain.

During the last cycle at $P_c = 120$ MPa, the behaviour of stress with strain is similar to that during the cycle at 20 MPa with an initial linear increase with total shortening leading to a deviation at 152 MPa, after which stress carries on increasing, albeit at a slower rate, up to its maximum value of 223 MPa. On the other hand, average local strain shows a linear increase with total shortening over the entire loading cycle with the exception of slight fluctuations towards the end of the cycle.

With increasing confining pressure from 20 to 120 MPa, the overall mechanical response of the faulted sample gradually evolves from the two extreme cases described above (highest and lowest tested confining pressures). For every cycle, we pick three stresses of interest: 1) the point at which stress exits linear elasticity or yield stress (σ_y); 2) the stress corresponding to the point where SGs and LVDTs data diverge, or in other words, the stress at which the fault reactivates (σ_f); and 3) the stress reached at the end of the loading cycle (σ_{max}), i.e., the sample maximum strength. These points are shown in Figure 2 to illustrate the picking process and otherwise compiled and plotted as a function of confining pressure for all three experiments in Figure 3 a., b. and c.

Under dry conditions, at a strain rate of 10^{-5} s^{-1}, yield stress σ_y and fault

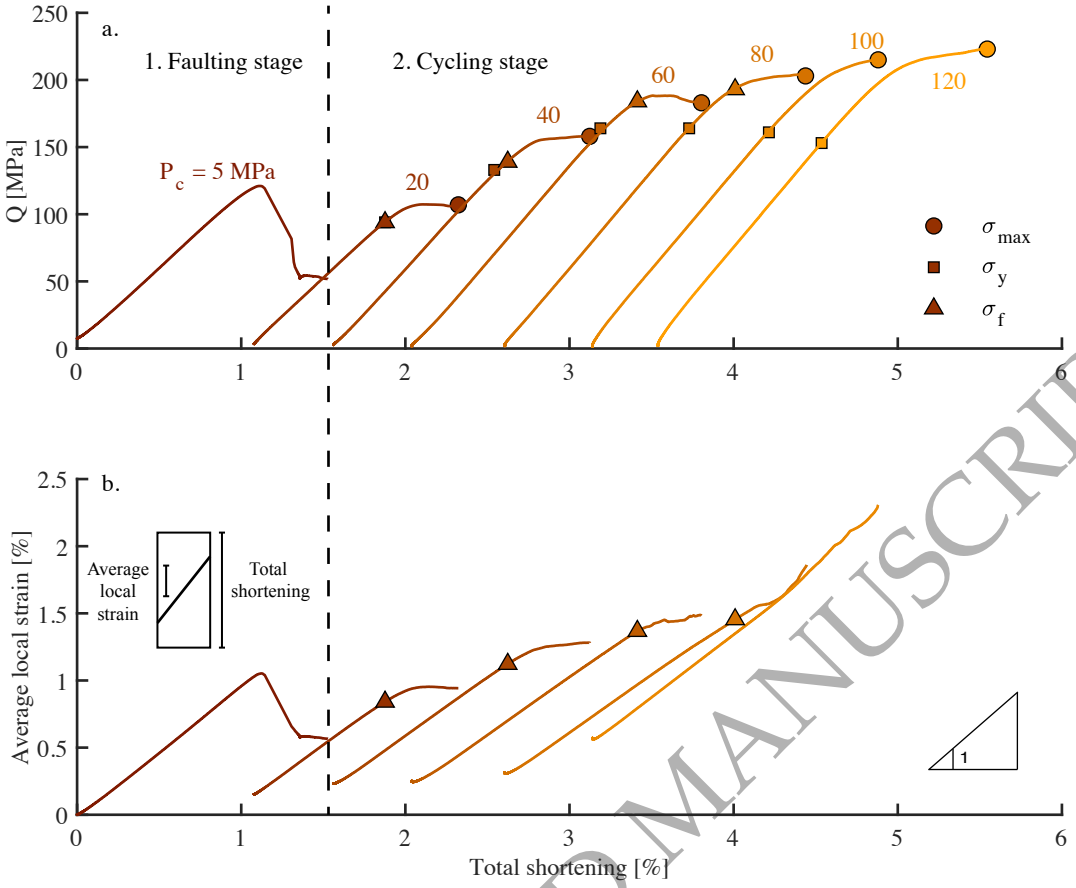

Figure 2: Mechanical data for the full experiment conducted dry at a strain rate of 10^{-5} s^{-1}. In a, Stress against total shortening (i.e., LVDT output). In b, Average local strain (i.e., averaged axial strain gauges outputs) against total shortening. For the sake of clarity, the unloading part of the curves have been left out. The circles represent the maximum stress reached during a loading cycle (σ_{max}), the squares represent the yield strength of the sample (σ_{y}) and the triangles represent the frictional strength of the fault (σ_{f}). Numbers above the curves denote the confining pressure in MPa. The inset in the top left corner of panel b is a schematic cross-section of the sample representing the different strain outputs plotted, and the inset in he bottom right is a visual cue for a slope of one.

strength σ_f are equal at $P_c = 20$ MPa (Figure 3 a.). Subsequently, yield strength increases with confining pressure up to a maximum of 160 MPa at $P_c = 80$ MPa. With further increase in P_c, yield strength slightly decreases and reaches 143 MPa at $P_c = 120$ MPa. The residual frictional strength after failure at $P_c = 5$ MPa is equal to 51 MPa. From there, it increases linearly with increasing confining pressure until it equates σ_{max} at a maximum of 200 MPa at $P_c = 80$ MPa. Beyond this point, σ_f could not be quantified anymore since no deviation between strain gauge and LVDT outputs was observed. The maximum strength increased, first rapidly from 107 MPa at $P_c = 20$ MPa to 200 MPa at $P_c = 80$ MPa, and then only showed a slight increase with confining pressure until it reached 213 MPa at $P_c = 120$ MPa. During the same experiment, at $P_c = 20$ MPa, the contribution of fault slip to the total deformation of the sample is about 80% (Figure 3 d.) With increasing confining pressure, this contribution gently decreases down to 60% at at $P_c = 60$ MPa. With a further increase in confining pressure of 20 MPa, the contribution of slip to the total deformation drops to 0% where it remained for all subsequent cycles. Under dry conditions and strain rate of 10^{-4} s^{-1}, the overall evolution of σ_y, σ_f and σ_{max} is similar to that described above, albeit with generally higher values. Initially, at $P_c = 20$ MPa, σ_y is equal to σ_f at $P_c = 20$ MPa at 94 MPa. It then reaches a maximum value of 187 MPa at $P_c = 100$ MPa and subsequently gently decreases to 142 at $P_c = 160$ MPa.

σ_f is equal to 50 MPa at $P_c = 5$ MPa. It then linearly reaches its maximum value of 226 MPa at $P_c = 100$ MPa before remaining somewhat constant at 215 up to $P_c = 160$ MPa. The maximum stress is equal to 115 MPa at $P_c = 20$ MPa and reaches a maximum of 250 MPa at $P_c = 140$ MPa. In this experiment, the contribution of slip to the overall shortening shows a negative trend with increasing confinement (Figure 3 e.). From its initial value of 70% at $P_c = 20$ MPa it slowly decreases to 33% at $P_c = 140$ MPa, but never fully vanishes.

Under wet conditions and strain rate of 10^{-5} s^{-1}, the overall mechanical behaviour remains similar but with generally lower critical stress values than in the previous two cases. While referring to this experiment, all values of confinement are given as effective, i.e., $P_{eff} = P_c - P_f$. Yield strength reached 100 MPa at $P_{eff} = 80$ MPa. Frictional strength increased from 43 MPa at $P_{eff} = 5$ MPa to its maximum of 160 MPa at $P_{eff} = 60$ MPa. Finally, flow strength reached 190 MPa at $P_{eff} = 100$ MPa. Interestingly the strength reduction between the wet and dry cases at identical strain rate remains relatively constant at all tested confining pressure. On average, σ_{max} in the wet case is 0.91 the dry value and σ_y wet is 0.82 that of the dry sample. These values are in good accordance with that of the uniaxial strength (essentially σ_{max} at $P_{eff} = 0$ MPa) reduction due to water weakening in volcanic rocks of 0.92 reported by Heap and Violay (2021). Under wet conditions, the drop of the slip

contribution to the overall shortening of the sample is much sharper than in the previous two cases (Figure 3 f.). Indeed, it drops from its initial value of 70% at $P_{\text{eff}} = 20$ MPa to 0% at $P_{\text{eff}} = 60$ MPa. Beyond this point, it was no longer possible to record fault slip.

4 Discussion

4.1 Strain partitioning at the LDT in porous rocks

Our experiments show that, at lower confining pressure, when fault strength is lower than the bulk yield strength (and therefore controls the onset of irrecoverable deformation), the vast majority of the deformation (70-80%) is accommodated by on-fault slip (Figure 3 d, e, f). Hence, the deformation can be considered localized. At the highest tested confining pressures, fault strength is greater than the maximum stress the bulk rock can support and therefore, the fault is locked: the deformation is fully ductile. In between these two end members, under confining pressure conditions where $\sigma_{\text{y}} < \sigma_{\text{f}} < \sigma_{\text{max}}$, the transition from purely localized to purely ductile deformation is progressive: this is the localized to ductile transition. This bounding criterion is identical to that found to control the LDT in marble (see Equation 1; Meyer et al. (2019)) which tend to show that, to the first order, the localized to ductile transition is similar in both porous and tight rocks despite their different porosities, microstructures

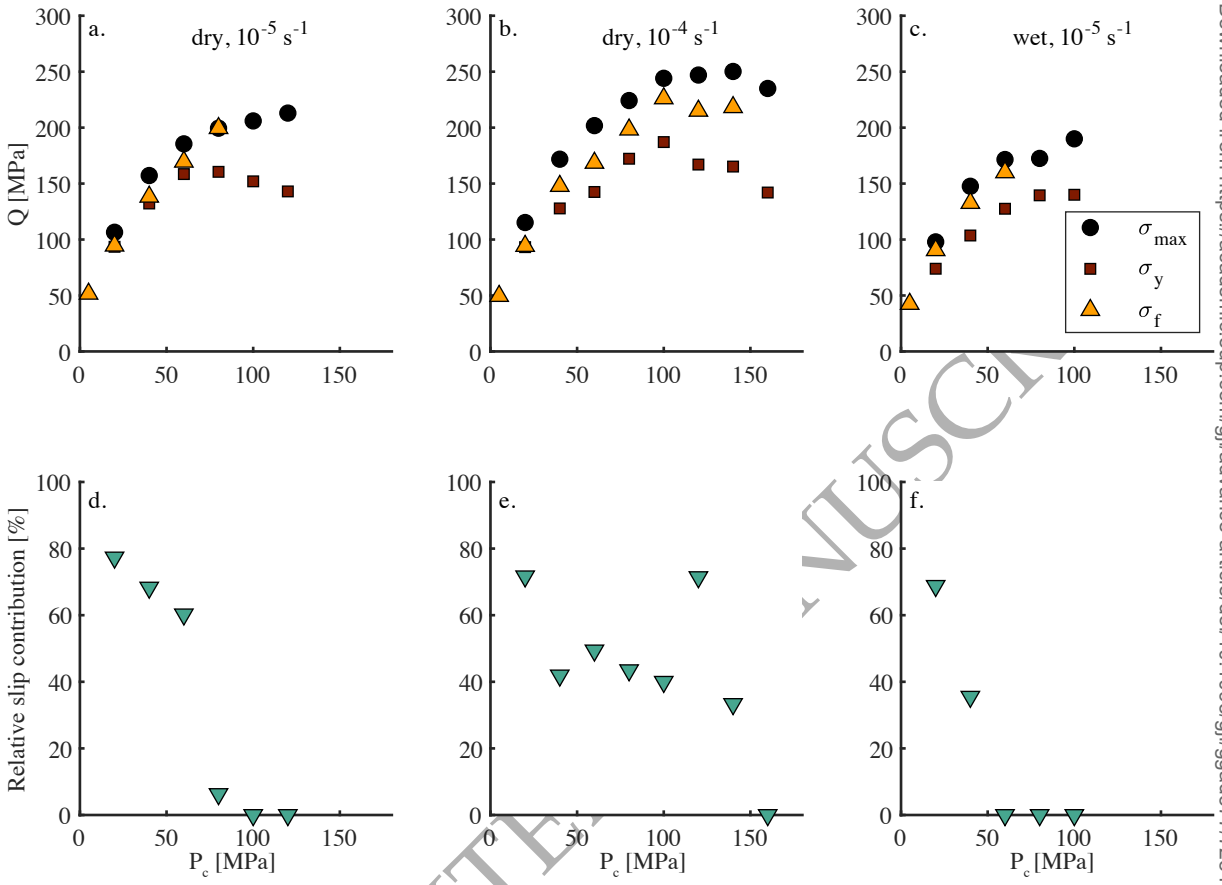

Figure 3: Maximum stress reached during loading (σ_{max}), sample yield strength (σ_{y}) and fault strength (σ_{f}) as well as slip contribution to the total deformation in a faulted sample of Volvic tranchyandesite through the BDT. Panels a-c: σ_{max} (circles), σ_{y} (squares), and σ_{f} (triangles) against confining pressure. Panels d-f: relative slip contribution to the total shortening against confining pressure.

and operative micromechanisms in the ductile regime.

In this intermediate regime, when a sample of Volvic tranchyandesite is loaded, strain is first accommodated elastically until the yield strength of the rock is reached. With further loading, strain is accommodated fully in the bulk before strain hardening eventually leads to fault reactivation. Once the fault has reactivated, the relative contribution of the two units (fault versus bulk rock) is controlled by the relative strength of the micro-processes controlling the deformation of these units (i.e., σ_{f} and σ_{y}). In other words, the greater fault strength is compared to the yield strength of the bulk, and the lower the contribution of fault slip to the total shortening of the sample will be.

To highlight the role of the different strengths in the partitioning of strain, we gather the slip contribution to the total shortening of the samples against the strength ratio $(\sigma_{\mathrm{f}} - \sigma_{\mathrm{y}})/(\sigma_{\mathrm{max}} - \sigma_{\mathrm{y}})$ in Figure 4. Within the LDT, after fault reactivation, the relative partitioning of strain between fault slip and off fault damage is inversely proportional to $(\sigma_{\mathrm{f}} - \sigma_{\mathrm{y}})/(\sigma_{\mathrm{max}} - \sigma_{\mathrm{y}})$ and thus, no matter the strain rate or presence of pore fluid. Even more striking is that rock type does not seem impact the relationship and both Carrara marble and Volvic trachyandesite follow the same trend, despite their vastly different composition, microstructure, etc. The data for Volvic tranchyandesite, despite being slightly more scattered are in very good accordance with the data gathered on Carrara marble by

Meyer et al. (2019). This accrued dispersion in the data of the present study can be explained by the occurrence of compaction bands as shown in the study of Heap et al. (2022). Indeed, if such a band was to from underneath a strain gauge, the sensor would record strain signals greater than the overall bulk strain. To alleviate this effect we never used data from a single sensor, but rather average outputs.

Under such a wide variety of conditions (fast vs slow deformation, wet vs dry, trachyandesite vs marble, etc) we expect the mechanisms controlling the different critical stresses to differ. In fact, it is well known that, in marble, yielding is controlled by plasticity (twinning; Fredrich et al. (1989)). On the other hand, as investigated by Heap et al. (2022) on samples originating from the same block, in the same machine and at the same conditions, at low pressure, yielding in Volvic tranchyandesite is controlled by micro-cracking and, at higher pressure, by cataclastic pore collapse. Similarly, we expect the presence of water in Volvic tranchyandesite to decrease both the yield and maximum strengths of the rock through the activation of chemical processes such as stress corrosion or the reduction of fracture toughness (Heap and Violay, 2021). Despite this fundamental differences in micro-mechanisms controlling the critical stresses, our empirical relationship describes strain partitioning. This is rooted in the phenomenological nature of the ratio. Once two deformation processes are active, it is the relative difference between their activation

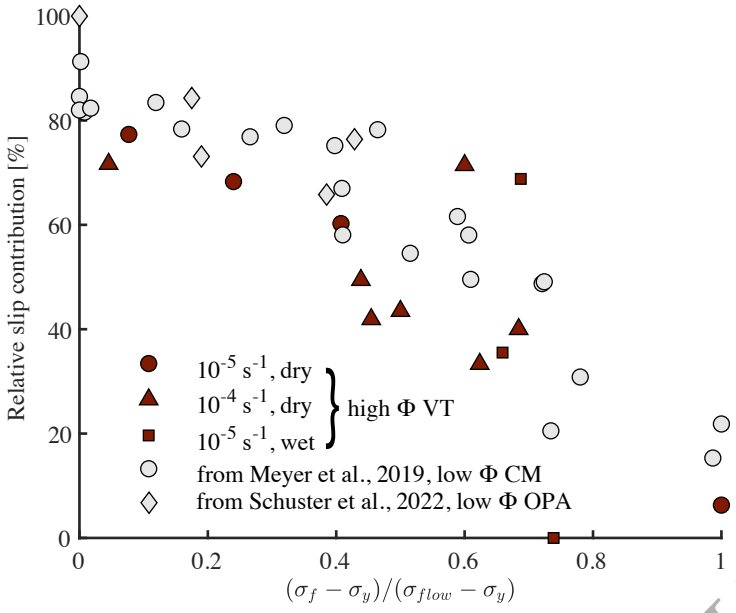

Figure 4: Relative slip contribution to the total shortening against the strength ratio $(\sigma_\mathrm{f} - \sigma_\mathrm{y})/(\sigma_\mathrm{max} - \sigma_\mathrm{y})$. Red data points were gathered in the present study while grey data points were gathered in the literature. VT: Volvic trachyandesite; CM: Carrara marble; OPA: Opalinus clay.

stresses (or strengths) that defines the partitioning rather than the nature of the processes itself. Interestingly, the existence of such strength ratios controlling partitioning has also been observed in models of viscous shear zones (Fagereng and Beall, 2021).

4.2 Critical stress envelope

The mechanical behaviour of porous rocks is usually considered in terms of a failure envelope and yield cap (Wong and Baud, 2012). In this representation, the possible stress states a porous rock can endure is

represented in P-Q space, where P is the effective mean stress (i.e., mean stress minus the pore pressure), and Q is the differential stress.

This envelope is built around two parts. Firstly, under low effective mean stress, porous rocks undergo dilatant permanent strain above a critical stress C', culminating in sample-scale failure when a critical peak stress is reached. This peak stress is what composes the failure envelope (C' not being systematically represented). At higher effective mean stress, applying a differential stress to a porous rock leads to compactant irrecoverable strain (a phenomenon referred to as shear-enhanced compaction Wong and Baud (2012)) beyond a critical yield stress value C*. This is what constitutes the yield cap. The failure envelope and the yield cap plotted together form what is usually referred to as envelope or cap. Given the "BDT" in porous rocks is defined as being the transition from cataclastic failure to compactant cataclastic flow, the intersection of these two parts of the curve (i.e., the summit of the cap) is considered a proxy of the transition and is often used to discriminate between "brittle" and "ductile" samples (rock rheology in this particular zone being mixed and, at times, extremely complex).

This representation raises a first concern in that the failure envelope is defined with two fundamentally different critical stresses, one being a stress at the onset of inelastic deformation or yield stress (σ_{y}) and the other being the maximum stress a rock can support (i.e., σ_{max}).

Moreover, these envelopes are established through testing initially intact rocks, however, in the crust, most of the tectonic strain is accommodated on inherited structures (preexisting faults and ductile shear zones). Hence, there is a need to account for the effect of preexisting features in rock envelopes.

In the light of our past experiments and those presented here, it is clear that describing the deformation of a rock through its ultimate mode of failure can be an oversimplification and multiple rheological transitions can occur leading to failure. For instance, at low P, in the brittle regime, failure in porous rocks is always preceded by some irrecoverable dilatancy (a statement that is also valid for tight rocks, but we will focus our discussion on porous rocks only). Given this dilatancy is a precursor to rock failure, the critical stress C' above which it occurs is below $\sigma_{\max}$ and marks the onset of irrecoverable deformation. Hence, it is necessary to systematically represent it in envelopes.

Similarly, at higher P, in the "ductile" regime, continuous loading has been observed to lead to a transition from compactant to dilatant cataclastic flow above a critical stress C*'(e.g., in Tavel and Indiana limestones, Vajdova et al. (2004), in Bentheim sandstone Wong and Baud (2012), in andesite Heap et al. (2015)). In some other cases, compactant flow could even lead to localized failure of the rock (Wong et al., 2001). Hence, a complete description of the macroscopic transition (LDT) or the

microscopic mechanism transition (compactant to dilatant) of a porous rock need to account for (when possible) other critical stresses than C*, such as C*'.

Here, we propose a thought experiment to see if it is possible to describe the localized to ductile transition of a faulted porous rock at a given temperature and strain rate using the same framework developed for tight rocks (Meyer et al., 2019) and accounting for all critical stresses (Figure 5). In order to give our representation a somewhat realistic scale, we base its shape on existing data for Volvic tranchyandesite found in the literature (Heap and Violay, 2021) as well as the data produced in the present study. These are gathered in Figure 5 a. and our synoptic model is drawn in Figure 5 b. We then expand the exercice to two other porous rocks, Bentheim sandstone (Baud et al., 2006) and Solnhofen limestone (Baud et al., 2000), to verify the applicability of our representation.

On the brittle side, the first element we draw is $\sigma_{\text{max dilatant}}$, the peak strength at failure for intact Volvic tranchyandesite (black in Figure 5 b.) We shape it following the failure envelope reported in Heap and Violay (2021). Since $\sigma_{\text{max dilatant}}$ is controlled by dilatant micro-cracking, it has a positive trend with effective mean stress which allow us to extrapolate its shape beyond the top of the cap reported by Heap and Violay (2021).

The second critical stress surface we plot in our model is that at the onset of dilation, C'(or dilational yield strength; dark blue in Figure 5 b.).

Depending on the failure criterion considered, C' can follow different shaped trend (e.g., linear with the Griffith's criterion), here, we assume a dependency similar to that of $\sigma_{\text{max dilatant}}$ since both stress surfaces are controlled by micro-cracking Wong et al. (1997); Vajdova et al. (2004)). Naturally, C' is always lower than $\sigma_{\text{max dilatant}}$. It is important to note here, that the data for C' in Figure 5 a. have been extracted from the stress-strain measurements reported in Heap and Violay (2021). It is common practice for porous rocks to pick C' using volumetric (or porosity change) plots coupled with acoustic emissions data, a method that usually yields values of C' lower (and more accurate) to those presented here. Despite this difference, we deem our determination method to be more suitable for this study, since it allows for a consistent source for all critical stresses used to build the failure envelope. Additionally, this method is that used in Meyer et al. (2019) which allows for direct comparison of the envelopes.

In the ductile regime, we draw C* (red in Figure 5 b.), which is the onset of compactive cataclastic flow (shear-enhanced compaction), or, in other words, the compactive yield strength. We use the second half of the envelope provided in Heap and Violay (2021) to estimate its amplitude and trend. Furthermore, Wong and Baud (2012) shows that C* is inversely correlated with P and that it is expected to intersect the x-axis of the P-Q diagram at a pressure P^* where inelastic compaction initiates under the

sole action of hydrostatic pressure.

Additionally, we hypothesize that there exists a maximum stress, $\sigma_{\text{max compactant}}$, a ductile rock can support or, in other words, a conceptual surface representing the strength at which the strongest pore in the rock will collapse (black in Figure 5 b.) We do not have data concerning such a critical stress. In fact, in the ductile regime, porous rocks tend to display continued strain hardening and it is common practice to consider rock strength to be that at an arbitrary value of strain beyond initial failure (e.g., 5%; Schock et al. (1973); Baud et al. (2006). This apparent "strength" is not what we desire to represent here, but we will use it as a proxy for the envelope. We expect it to have a dependency to P similar to that of C*, since both are controlled by the same micro-processes (pore collapse and/or grain crushing). Being the maximum stress the pore structure in a ductile rock can possibly bear, it will always be above C*. Finally, since our experiments were carried on faulted rocks, we are able to add fault strength in our model. In the vast majority of cases, for crustal rocks, fault friction is linearly correlated to effective mean stress with a slope corresponding to the static friction coefficient of the fault (often between 0.4 and 0.7) (Byerlee, 1968). In our diagram, we set the slope of σ_{f} to match our fault reactivation data.

Now that the main units of our representation are in place, we can shift our attention to its implications. First and foremost, the LDT as defined

by the criteria discussed in Section 4.1 is much wider than the previously accepted "BDT" in porous rocks. For example, in dry Volvic trachyandesite deformed at 10^{-5} s^{-1}, it spans 80 to 130 MPa in confinement. It arises that there exists an entire stress regime were compactive cataclastic flow can lead to fault reactivation provided the sample undergoes strain hardening (dark grey area in figure 5 b.) In other words, in this zone, continuous deformation of a porous rock would sequentially lead to it being ductile (possibly generating compaction bands) before leading to failure along a fault.

We expect the intersection of the two critical yield stresses (dilatant C' and compactant C*) to mark an abrupt switch from one yielding micro-mechanism to the other. While it does not bear implication for the localized or ductile nature of strain on a macroscopic scale, it marks a sharp, well-defined boundary, as opposed to the current "top of the cap" criterion that only gives an approximate zone for the "BDT". For this reason, the authors would like to encourage its use as a proxy for the colloquial "BDT" as well as a sharp boundary for the dilatant to compactant transition (DCT).

In our representation, and in good accordance with experimental observations reported earlier, there exists a stress regime where C' is greater than C*, but not yet above $\sigma_{\max}$. This is the condition under which a transition from compactant to dilatant cataclastic flow through

strain hardening can occur (C*'). While we cannot constrain the extent of this regime in P-Q space from our data, we can hypothesize that it will be controlled by the relative amplitude of C' and C* (i.e., the relative position of the two stress surfaces with respect to one another). Naturally, under specific circumstances, the opposite case should exist in certain rocks (i.e., dilatant to compactant cataclastic flow, C'*).

Overall, our failure envelope model restricts the possible stress states a faulted rock can experience (light grey area in Figure 5 b.) Firstly, in the cataclastic, localized regime, it is "smaller" than that for intact rocks, since the maximum stress a rock can sustain is controlled by the strength of the fault.

Within the LDT, the maximum strength is still controlled by fault strength, but a significant amount of strain hardening is necessary to reach fault reactivation from the yielding point (C' in this representation).

The LDT is achieved as the fault strength equates that of the rock maximum strength; the rock is fully ductile - no localization on a fault can occur. In this regime, there can still exist a switch from compaction to dilation, depending on the values of the two critical stress C* and C' respectively.

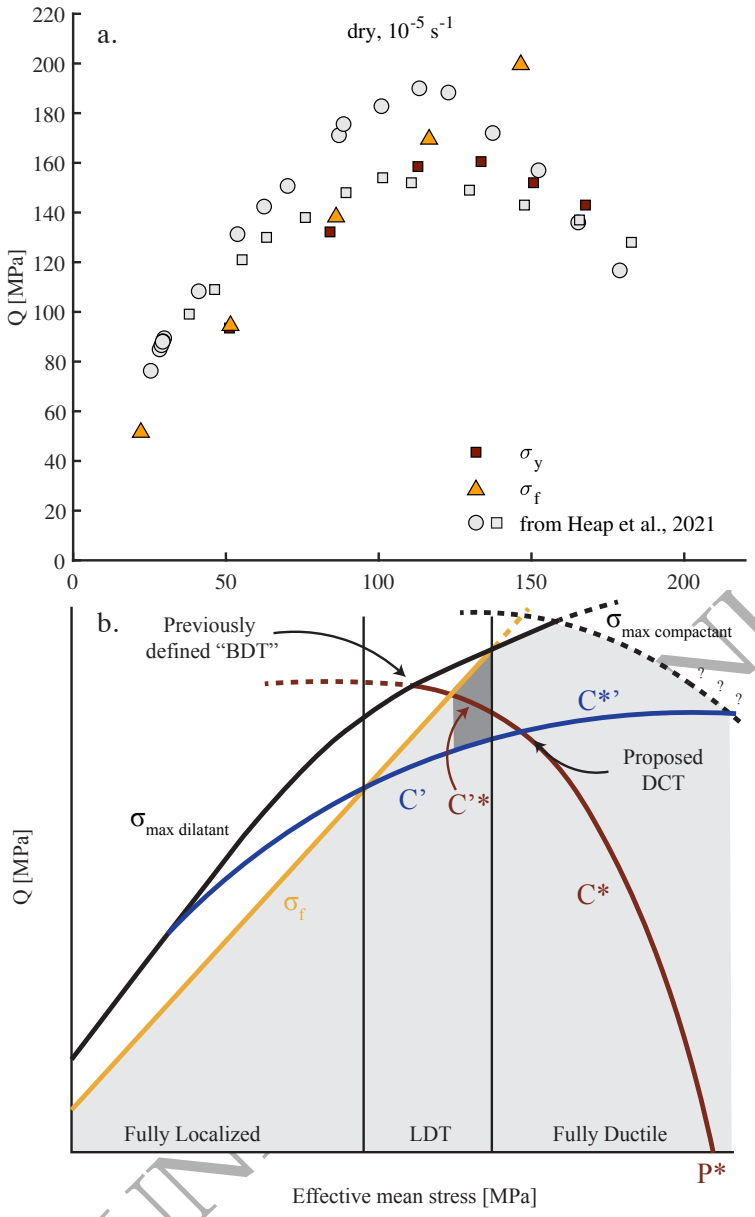

Figure 5: (a.) Volvic trachyandesite critical stresses data gathered in the present study (coloured) and from Heap and Violay (2021) (grey) against effective mean stress. (b.) Critical stress envelope representation. The light grey area represent possible stress states in a faulted porous rock and the dark grey area represents stress states where compaction banding can lead to fault reactivation. Question marks denote a curve that is not based on any existing data.

4.3 Implications for porous rocks and reservoirs

In this study, we deformed a porous volcanic rock that is not necessarily representative of reservoir rocks (geothermal, oil or aquifers) which tend to be hosted in sandstone or limestone. Moreover, the critical stresses used to build the representation discussed in the previous section are controlled by micro-mechanical processes (e.g., microcracking for C', grain crushing or pore collapse for C*) which are themselves controlled by intrinsic properties of the rocks such as mineralogy, porosity, anisotropy, etc. Hence, the absolute values, but also the trends followed by the different critical stresses $\sigma_{\text{max dilatant}}$, $\sigma_{\text{max compactant}}$, σ_{f}, C' and C* with P will be highly sensitive to rock type and one can wonder whether our critical stress envelope is suitable to describe the LDT in other, more standard, porous rocks. In order to validate our representation, we will try to apply it to different rock types in the following section.

For this study, we were granted full access to the mechanical data presented in Baud et al. (2006) and Baud et al. (2000), two studies that thoroughly investigated the mechanical behaviour of Bentheim sandstone and Solnhofen limestone respectively, through the BDT. These two rocks are well studied and give us insights into the rheology of sandstones and limestones, two major porous rock types aside from lavas.

We retraced the original stress-strain curves and picked the critical stresses following the method we applied on our own data. Where volumetric

strain data were available, we used it to discriminate dilatant or compactant yielding, in other words, we used the pore volume data to discriminate between C' and C*. In the case of Solnhofen limestone, we also used the volumetric strain data to pick C*' since it is not possible to do so using axial strain only. Similarly, in Bentheim sandstone, we picked C'* using volumetric data. Where possible, we used the residual friction (i.e., sample strength after brittle failure) to plot σ_{f}. For both rocks, $\sigma_{\mathrm{max\ compactant}}$ was picked at 5% axial strain. The resulting critical stress envelopes along with the envelope built in the previous section for Volvic trachyandesite are shown in Figure 6.

The critical stress envelope of Bentheim sandstone appears similar to that of Volvic trachyandesite to the first order, albeit much "wider" (Figure 6 b.). In this case, the LDT initiates around $P = 60$ MPa, where σ_{f} equates C' and terminates around $P = 160$ MPa, where σ_{f} equates $\sigma_{\mathrm{max\ dilatant}}$. C' and C* intersect around $P = 200$ MPa (micro-mechanical yielding transition or DCT), implying that, throughout the entire LDT, yielding in Bentheim sandstone is controlled by dilatant micro-cracking. At $P = 110$ MPa and $P = 130$ MPa, we observed compaction prior to failure and above C', i.e., C'*.

The critical stress envelope of Solnhofen limestone appears widely different than the previous 2 (Figure 6 c.) In this case, no residual friction data were available, hence, it is impossible to bound the LDT. In this rock, the

micromechanical yielding transition occurs around $P = 200$ MPa. Beyond this point, dilatant deformation is observed above C* up until about $P = 500$ MPa, where C*' intersects $\sigma_{\text{max compactant}}$. At this point, the rock is unable to undergo dilatancy.

The two critical stress envelopes are in good accordance with experimental and post-mortem observations of the sample both for sandstone and limestone. It describes accurately the LDT in the case of Bentheim sandstone as well as dilatant to compactant transition in both rocks. The stark difference in appearance of the envelopes can be attributed to the difference in intrinsic rock properties and, for this reason, a critical stress envelope can be considered a rock's rheological fingerprint. For this same reason, and for a given rock type, numerous external factors such as, presence of fluids, strain rate, temperature, etc can impact some or all critical stresses, moving the lines within the critical stress envelope as demonstrated by our experiments on Volvic trachyandesite (Figure 3 c., f.). However, despite these fundamental differences, the relationship between the critical stresses of a given rock in a given state appear to always describe accurately the initiation and termination of the LDT (i.e., its boundaries) as well as the partitioning of strain (Figure 4).

Furthermore, it is clear that one main controls of crustal rock rheology is strain hardening. The ability of a rock to sustain a high degree of hardening when strained will control whether the rock can activate several

deformation mechanisms sequentially and how much strain will be necessary to do so; in other words, in the critical stress envelope representation, strain hardening will control the loading path in P-Q space and how many critical stress lines can be crossed. It is now crucial to better understand strain hardening and its mechanisms in the crust to fully capture the behaviour of porous rocks.

Our results show that the LDT is far more extended than previously believed and that it could initiate at depth as shallow as 1-2 km given most reservoirs are already faulted. Such a wide LDT implies that the complex transitional rheology might occur in reservoir rocks over a wide spectrum of P, T. This can make designing and modelling safe and efficient extraction or injection operations challenging.

For instance, in brittle reservoirs, faults can be targeted for stimulation since shear reactivation can improve their permeability and the economic potential of the rock mass (Carey et al., 2015; Wenning et al., 2019), but these processes can lead to substantial induced seismicity. On the other hand, ductile reservoirs are usually considered aseismic, but diffuse deformation and the formation of compaction bands lead to permeability reductions (e.g. in Volvic trachyandesite, Heap et al. (2022)) and hence to a decrease in productivity of the reservoir. The existence of a stress state where both fault slip and compactive cataclastic flow coexist bears implication for the engineering of reservoirs as it could mean that

permeability in ductile reservoirs could be improved, but at the same time that ductile reservoirs, considered seismically inactive, could host induced earthquakes if strain hardening accompanying ductile deformation leads to fault reactivation.

Additionally, we showed that in the LDT, different deformation mechanisms can occur sequentially or concurrently. At the scale of the reservoir, this could imply that the global response of the rock mass to injection or extraction operations could change over the lifetime of the exploitation, drastically changing its productivity and/or safety.

Similarly, given the wide array of literature available on the effect of external factors such as mineralogy, presence of water, stress, temperature, etc., on σ_{y} and σ_{max} in both the brittle and ductile regimes, we expect the LDT to demonstrate a high degree of sensitivity to these factors. Hence, a reservoir geomechanical properties such as strength, stiffness, etc, could vary in response to stress changes induced by exploitation. For example, a reservoir rock could become ductile after extended exploitation and become too weak to support the overburden, leading to subsidence or collapse of the reservoir.

Overall, the consequences of a wide LDT on the mechanical behavior of geo-reservoirs is complex and depend on numerous factors. Therefore, it is important to account the LDT and its extent when evaluating the geomechanical properties and behaviour of a reservoir.

Finally, and from a more speculative stand-point, given how the strain partitioning relationship described by Equation 2 seems to remain valid regardless of rock-type (Figure 4), and given the similar ratio found by Fagereng and Beall (2021) for modelled viscous shear-zones, one can wonder whether strain partitioning between two given deformation mechanisms can be estimated through a ratio of their respective activation critical stress. If this were to be true, a critical stress envelope would, in addition to map a rock rheology, map the partition of strain among active deformation mechanisms at any given stress state.

5 Conclusion

We explored the brittle to ductile transition of porous rocks, one of the most important for human society yet poorly understood crustal unit. We demonstrated the existence of the localized-ductile transition in faulted Volvic trachyandesite, and by extension, in faulted porous rocks. We showed that this transition initiates at confining pressures lower than previously accepted for the colloquial "brittle-ductile transition". Our observations suggest that the LDT in the crust could occur at very shallow depth (1-2 km). Within the LDT, strain partitioning follows the empirical law established previously for tight rocks, regardless of the deformation micro-mechanisms involved, and that, under certain circumstances, compactant cataclastic flow (compaction bands) can lead to fault

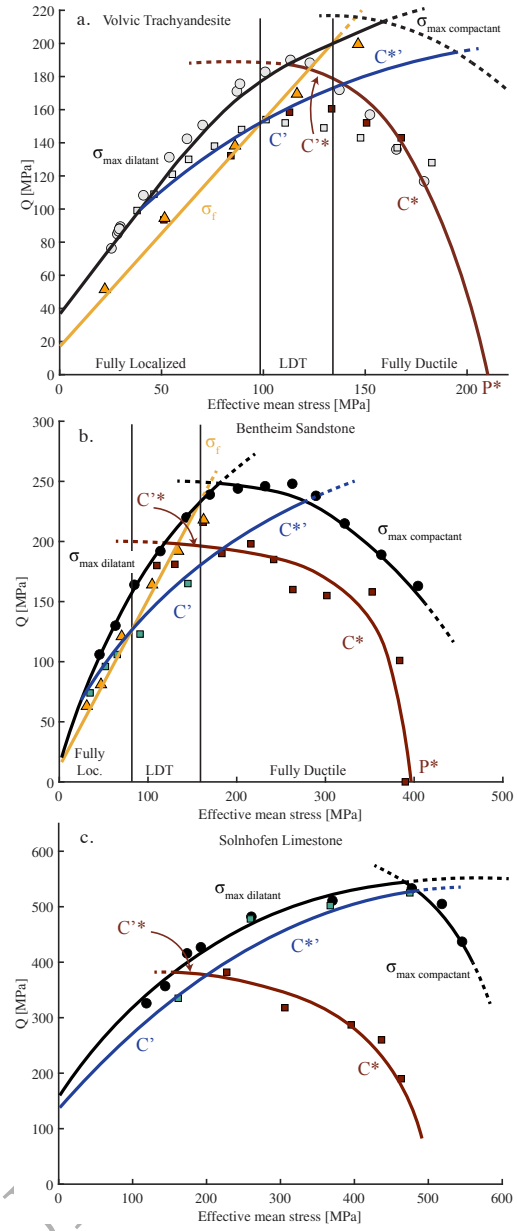

Figure 6: In a, Volvic trachyandesite critical stresses data gathered in the present study (coloured) and from Heap and Violay (2021) (grey) against effective mean stress. along with the critical stress envelope representation (see Figure 5 for details). Critical stress envelope of Bentheim sandstone (b.) and Solnhofen limestone (c.) All data were picked in the framework of this study on the original data of Baud et al. (2006) and Baud et al. (2000) for Bentheim sandstone and Solnhofen limestone respectively.

reactivation. Our findings suggest that georeservoirs of ductile rocks are prone to reactivated seismicity. Furthermore, ductile reservoirs could be stimulated along frictional faults. Moreover, we elaborate on a new representation of critical stress envelopes. By mapping the activation stresses of the deformation mechanisms (C' and C*), as well as the maximum strength of these processes (σ_{f}, $\sigma_{\text{max dilatant}}$, and $\sigma_{\text{max compactant}}$) of a rock mass with discontinuties, we represent the rheology of three porous rocks, namely Volvic trachyandesite, Bentheim sandstone and Solnhofen limestone. Within the framework of this representation, we proposed a new criterion for the colloquial "BDT" based on the transition in yielding micro-mechanisms (from dilatant to compactant yielding, i.e., C' to C*). We speculated that such a representation could allow for the mapping of strain partitioning between individual micro-processes within crustal rocks.

6 Acknowledgements

The authors would like to express their gratitude to Prof. Patrick Baud for having generously provided parts of the data that supported this study as well as for their insightful advices. The authors would also like to thank Prof. Michael Heap for fruitful conversations on the topic of the BDT. The authors extend their gratitude to Anne Pluymakers and an anonymous reviewer for their insightful contributions. This project has received

fundings from the European Research Council Starting Grant project 757290-BEFINE.

7 Author contributions

GM designed and carried-out the experiments. GM processed data and elaborated the models. All authors participated in the discussion as well as the redaction of the manuscript.

The authors declare no competing interest.

8 Data availability statement

The data produced in the framework of this study are available at Zenodo repository via https://doi.org/10.5281/zenodo.7767636

References

Antonellini, M. and Aydin, A. (1994). Effect of faulting on fluid flow in porous sandstones: petrophysical properties. *AAPG bulletin*, 78(3):355–377.

Aydin, A. and Johnson, A. M. (1978). Development of faults as zones of deformation bands and as slip surfaces in sandstone. *Pure and applied Geophysics*, 116:931–942.

Baud, P., Schubnel, A., and Wong, T.-f. (2000). Dilatancy, compaction, and failure mode in Solnhofen limestone. *Journal of Geophysical Research: Solid Earth*, 105(B8):19289–19303.

Baud, P., Vajdova, V., and Wong, T.-f. (2006). Shear-enhanced compaction and strain localization: Inelastic deformation and constitutive modeling of four porous sandstones. *Journal of Geophysical Research: Solid Earth*, 111(B12).

Brantut, N., Heap, M. J., Baud, P., and Meredith, P. G. (2014). Rate-and strain-dependent brittle deformation of rocks. *Journal of Geophysical Research: Solid Earth*, 119(3):1818–1836.

Byerlee, J. D. (1968). Brittle-ductile transition in rocks. *Journal of Geophysical Research*, 73(14):4741–4750.

Carey, J. W., Lei, Z., Rougier, E., Mori, H., and Viswanathan, H. (2015). Fracture-permeability behavior of shale. *Journal of Unconventional Oil and Gas Resources*, 11:27–43.

Coelho, L. C., Soares, A. C., Ebecken, N. F. F., Alves, J. L. D., and Landau, L. (2005). The impact of constitutive modeling of porous rocks on 2-D wellbore stability analysis. *Journal of Petroleum Science and Engineering*, 46(1-2):81–100.

Cornelio, C. and Violay, M. (2020). Effect of Fluid Viscosity on Earthquake Nucleation. *Geophysical Research Letters*, 47(12):e2020GL087854.

Fagereng, . and Beall, A. (2021). Is complex fault zone behaviour a reflection of rheological heterogeneity? *Philosophical Transactions of the Royal Society A: Mathematical, Physical and Engineering Sciences*, 379(2193):20190421.

Fisher, Q. J., Casey, M., Clennell, M. B., and Knipe, R. J. (1999). Mechanical compaction of deeply buried sandstones of the North Sea. *Marine and Petroleum Geology*, 16(7):605–618.

Fowles, J. and Burley, S. (1994). Textural and permeability characteristics of faulted, high porosity sandstones. *Marine and Petroleum Geology*, 11(5):608–623.

Fredrich, J. T., Arguello, J. G., Deitrick, G. L., and de Rouffignac, E. P. (2000). Geomechanical modeling of reservoir compaction, surface subsidence, and casing damage at the Belridge diatomite field. *SPE Reservoir Evaluation & Engineering*, 3(04):348–359.

Fredrich, J. T., Evans, B., and Wong, T.-F. (1989). Micromechanics of the brittle to plastic transition in Carrara marble. *Journal of Geophysical Research: Solid Earth*, 94(B4):4129–4145.

Grigoli, F., Cesca, S., Priolo, E., Rinaldi, A. P., Clinton, J. F., Stabile,

T. A., Dost, B., Fernandez, M. G., Wiemer, S., and Dahm, T. (2017). Current challenges in monitoring, discrimination, and management of induced seismicity related to underground industrial activities: A European perspective. *Reviews of Geophysics*, 55(2):310–340.

Heap, M. J., Farquharson, J. I., Baud, P., Lavalle, Y., and Reuschl, T. (2015). Fracture and compaction of andesite in a volcanic edifice. *Bulletin of Volcanology*, 77(6):55.

Heap, M. J., Meyer, G. G., Nol, C., Wadsworth, F. B., Baud, P., and Violay, M. E. S. (2022). The Permeability of Porous Volcanic Rock Through the Brittle-Ductile Transition. *Journal of Geophysical Research: Solid Earth*, 127(6):e2022JB024600.

Heap, M. J. and Violay, M. E. (2021). The mechanical behaviour and failure modes of volcanic rocks: a review. *Bulletin of Volcanology*, 83(5):33.

Jefferd, M., Brantut, N., Meredith, P. G., Mitchell, T. M., and Plmper, O. (2021). Compactive Deformation of Sandstone Under Crustal Pressure and Temperature Conditions. *Journal of Geophysical Research: Solid Earth*, 126(4):e2020JB020202.

Louis, L., Baud, P., and Wong, T.-F. (2007). Characterization of pore-space heterogeneity in sandstone by X-ray computed tomography. *Geological Society, London, Special Publications*, 284(1):127–146.

Makowitz, A. and Milliken, K. L. (2003). Quantification of brittle deformation in burial compaction, Frio and Mount Simon Formation sandstones. *Journal of Sedimentary Research*, 73(6):1007–1021.

Meyer, G. G., Brantut, N., Mitchell, T. M., and Meredith, P. G. (2019). Fault reactivation and strain partitioning across the brittle-ductile transition. 47(12):1127–1130.

Nol, C., Passelgue, F. X., Giorgetti, C., and Violay, M. (2019). Fault reactivation during fluid pressure oscillations: Transition from stable to unstable slip. *Journal of Geophysical Research: Solid Earth*, 124(11):10940–10953.

Nol, C., Passelgue, F. X., and Violay, M. (2021). Brittle faulting of ductile rock induced by pore fluid pressure build-up. *Journal of Geophysical Research: Solid Earth*, 126(3):e2020JB021331.

Paterson, M. S. and Wong, T.-F. (2005). *Experimental Rock Deformation - The Brittle Field*. Springer Science & Business Media.

Rutter, E. H. (1986). On the nomenclature of mode of failure transitions in rocks. *Tectonophysics*, 122(3-4):381–387.

Schock, R. N., Heard, H. C., and Stephens, D. R. (1973). Stress-strain behavior of a granodiorite and two graywackes on compression to 20

kilobars. *Journal of Geophysical Research (1896-1977)*, 78(26):5922–5941.

Scholz, C. H. (2019). *The mechanics of earthquakes and faulting.* Cambridge university press.

Schultz, R., Skoumal, R. J., Brudzinski, M. R., Eaton, D., Baptie, B., and Ellsworth, W. (2020). Hydraulic fracturing-induced seismicity. *Reviews of Geophysics*, 58(3):e2019RG000695.

Scott, T. E. and Nielsen, K. C. (1991). The effects of porosity on the brittle-ductile transition in sandstones. *Journal of Geophysical Research: Solid Earth*, 96(B1):405–414. Publisher: Wiley Online Library.

Shipton, Z. K. and Cowie, P. A. (2001). Damage zone and slip-surface evolution over m to km scales in high-porosity Navajo sandstone, Utah. *Journal of Structural Geology*, 23(12):1825–1844.

Tullis, J. and Yund, R. (1992). The brittle-ductile transition in feldspar aggregates: an experimental study. In Evans, B. and Wong, T.-f., editors, *International Geophysics*, volume 51 of *Fault Mechanics and Transport Properties of Rocks*, pages 89–117. Academic Press.

Underhill, J. R. and Woodcock, N. H. (1987). Faulting mechanisms in high-porosity sandstones; new red sandstone, Arran, Scotland. *Geological Society, London, Special Publications*, 29(1):91–105.

Vajdova, V., Baud, P., and Wong, T.-f. (2004). Compaction, dilatancy, and failure in porous carbonate rocks. *Journal of Geophysical Research: Solid Earth*, 109(B5).

Veeken, C. A. M., Walters, J. V., Kenter, C. J., and Davies, D. R. (1989). Use of plasticity models for predicting borehole stability. In *ISRM International Symposium*. OnePetro.

Wenning, Q. C., Madonna, C., Kurotori, T., and Pini, R. (2019). Spatial Mapping of Fracture Aperture Changes With Shear Displacement Using X-ray Computerized Tomography. *Journal of Geophysical Research: Solid Earth*, 124(7):7320–7340.

Wong, T.-f. and Baud, P. (2012). The brittle-ductile transition in porous rock: A review. *Journal of Structural Geology*, 44:25–53.

Wong, T.-f., Baud, P., and Klein, E. (2001). Localized failure modes in a compactant porous rock. *Geophysical Research Letters*, 28(13):2521–2524.

Wong, T.-f., David, C., and Zhu, W. (1997). The transition from brittle faulting to cataclastic flow in porous sandstones: Mechanical deformation. *Journal of Geophysical Research: Solid Earth*, 102(B2):3009–3025.

Yarushina, V. M. and Podladchikov, Y. Y. (2010). Plastic yielding as a

frequency and amplitude independent mechanism of seismic wave attenuation. *Geophysics*, 75(3):N51–N63.